Journal of Medical Imaging

MedicalImaging.SPIEDigitalLibrary.org

Classification of reticular pattern and streaks in dermoscopic images based on texture analysis

Marlene Machado
Jorge Pereira
Rui Fonseca-Pinto

SPIE.

Classification of reticular pattern and streaks in dermoscopic images based on texture analysis

Marlene Machado,[a] Jorge Pereira,[a] and Rui Fonseca-Pinto[a,b,*]
[a]Instituto de Telecomunicações, Multimedia Signal Processing Group, Morro do Lena, Alto do Vieiro, Campus 2, IPLeiria, Leiria 2411-901, Portugal
[b]Polytechnic Institute of Leiria, School of Technology and Management, Morro do Lena, Alto do Vieiro, Campus 2, Apartado 4163, Leiria 2411-901, Portugal

Abstract. The early detection of melanoma is one of the greatest challenges in clinical practice of dermatology, and the reticular pattern is one of the most important dermoscopic structures to improve melanocytic lesion diagnosis. A texture-based approach is developed for the automatic detection of reticular patterns, whose output will assist clinical decision-making. Feature selection was based on the use of two algorithms by means of the classical graylevel co-occurrence matrix and Laws energy masks optimized on a set of 104 dermoscopy images. The AdaBoost (adaptive boosting) approach to machine learning was used within this strategy. Results suggest superiority of LEM for reticular pattern detection in dermoscopic images, achieving a sensitivity of 90.16% and a specificity of 86.67%. The use of automatic classification in dermoscopy to support clinicians is a strong tool to assist diagnosis; however, the use of automatic classification as a complementary tool in clinical routine requires algorithms with high levels of sensitivity and specificity. The results presented in this work will contribute to achieving this goal. [DOI: 10.1117/1.JMI.2.4.044503]

Keywords: pattern recognition; melanoma; reticular pattern; dermoscopy.

Paper 15105RR received May 19, 2015; accepted for publication Nov. 30, 2015; published online Dec. 29, 2015.

1 Introduction

Melanoma is the skin cancer derived from melanocytes, cells that produce melanin (the skin coloration pigment). Despite being the least common among all skin cancers, melanoma is the deadliest form of the disease.[1] Due to the high malignancy potential of melanoma, the early detection of suspicious skin lesions is critical to prevent malignancy and to increase treatment efficacy.[2]

Dermoscopy is a noninvasive imaging technique used to obtain digital images on the surface of the skin using a device known as dermoscope (or dermatoscope). It uses a magnifying lens and a source light attached to a digital camera. This device allows the visualization of pigmented structures or vessels in the epidermis and superficial dermis.[3] Digital image processing applied to dermoscopic images is an important tool to improve medical evaluation, increasing the diagnosis sensitivity and specificity.[4–6] The use of image processing techniques allows preprocessing (enhancing contrast, alignment, etc.), elimination of common artifacts,[7–11] and extraction of quantitative features for structure classification,[5,12] and establishes a measure of malignancy associated with the lesion, as proposed in Refs. 13–18. These techniques also permit the use of automated classification of skin lesions, which is a valuable help to clinical practice.[19,20] In fact, one of the greatest challenges in classification is the higher inter- and intraindividual variability, due to the limited capacity of the human eye (contrast sensitivity, wavelength sensitivity, orientation discrimination, etc.).[21–23]

The pigmented network or reticular pattern and streaks are important diagnostic clues, representing a dermoscopic hallmark of melanocytic lesions, which is independent of their biologic behavior.[24] The reticular pattern appears as a grid of thin brown lines over a diffuse light-brown background. This is a honeycomb-like structure, consisting of round pigmented lines and lighter hypopigmented holes, forming a subtle pattern that appears in many melanocytic lesions. This pigmented distribution is arranged in keratinocytes, or along the dermoepidermal junction along the rete ridge, forming the observed pattern at the outer layer of the skin.

Streaks are brownish-black linear structures of variable thickness. These skin structures may have regular or irregular shapes, and they can be convergent or nonconvergent, but they are usually more visible when located at the periphery of the lesion. Some examples of these pigmented networks are shown in Fig. 1.

The evaluation of skin melanocytic lesions by dermatologists is performed upon a detailed observation of explicit features; this allows the use of specific algorithms for decision-making. In the most widely used algorithms (i.e., ABCD rule[25,26] and Menzies method[8,25]), the presence of a pigmented network is evaluated to calculate a malignancy index. Beyond the presence of a pigmented network, some works use the geometry and the change in the network to differentiate between benign and malignant melanocytic proliferations, which allows for a so-called typical or atypical network classification.[26]

2 Related Work

The importance of early detection of skin cancer, and the complexity of the clinical decision regarding the nature of the lesion, led in the last decade to the appearance of several works on the automatic detection of pigmented networks, whose contribution is very useful to enhance clinical classification by

*Address all correspondence to: Rui Fonseca-Pinto, E-mail: rui.pinto@ipleiria.pt

2329-4302/2015/$25.00 © 2015 SPIE

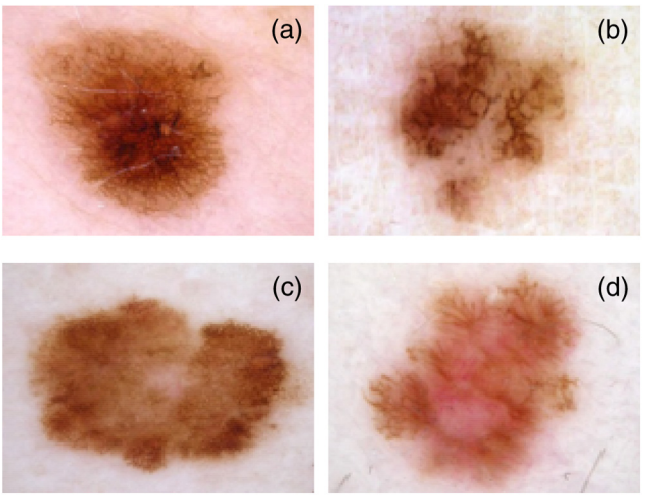

Fig. 1 Examples of reticular pattern in dermoscopy images: (a) Clark nevi, (b) congenital pseudomelanoma, (c) melanoma, and (d) melanoma with streaks.

dermatologists. Automated detection of the pigmented network is often a challenging problem, because in these reticular structures, there is a low contrast between the network and the background. In particular, the size of the net holes may comprise different shapes in different images and irregularities in their shape and size may often exist in the same image.

The approach proposed by Fleming et al.[27] aims to characterize pigmented networks using principles of differential geometry by measuring structural properties. This algorithm uses a process for the detection of curvilinear structures using the information obtained by the first and second derivatives. Ridge points (line centers) are identified with the ones that have a first derivative close to zero and a high second derivative in the perpendicular direction to the line. The final network is obtained by linking ridge points. The process of using second derivatives gives information about the orientation of the line and also about the closeness between network points. These set of lines establish the skeleton of pigmented network, and they are used to evaluate structural properties, such as the size of holes or the thickness of lines.

Anantha et al.[28] proposed two texture analysis algorithms: the first one using a neighborhood graylevel dependence matrix, and the second by applying Laws energy masks (LEM), whose performance has been proved to be higher than the previous one.

Grana et al.[4] established a similar methodology as in Ref. 2. However, they use morphological masks to perform the completion of the line, followed by a classification according to the distribution of the pigmented network, using the label "no network" in the case where no pigmented network is present, "partial network" if the lesion is partially covered with a pigmented network, and "complete network" otherwise.

The algorithms proposed by Betta et al.[29] and Leo et al.[30] are similar and they combine both structural and spectral techniques to perform the detection of pigmented networks. By using these algorithms, lines or points are simple shapes that can form a texture, and the authors used the structural technique to search for these forms. These configurations can identify local discontinuities by comparing the original graylevel image with its version obtained by a median filter followed by a close-opening operation, which removes some isolated points. The spectral technique is implemented in order to ignore the local discontinuities, which are not clearly associated with a network. This technique is based on Fourier analysis of the graylevel image and comprises a sequence of the fast Fourier transform, high-pass filtering, inverse fast Fourier transform, and thresholding. The results of both techniques are combined to provide a network image, in which the lesion area with pigmented network is highlighted. Leo et al.[30] include a final stage in the process, where the network itself is classified as "atypical" or "nonatypical," by selecting features from the image and using them in a decision classifier.

Sadeghi et al.[31] also presented an algorithm where the detection of network holes is performed. The algorithm comprises three steps. In the first one, sharp changes of intensity are detected using the Laplacian of Gaussian filter. Second, the result of this edge detection step is subsequently converted into a graph to find meshes or cyclic structures of the lesion. Finally, in the third step, after finding cyclic subgraphs of the graph, noise or undesired cycles are removed, and the pigmented network is created using the extracted cyclic structures. This graph is used for the detection of pigmented networks in a given image using a density ratio. According to the density of the pigmented network graph, the given image is classified into a "present" or "absent" network pattern.

The algorithm proposed by Barata et al.[32] establishes the detection of pigmented networks using a bank of directional filters and comprises three steps. First, the preprocessing is performed in order to remove possible artifacts as hair and light reflections. Then, regions with pigmented networks are detected using intensity and spatial organization. The intensity property is used to perform an enhancement of the network by applying a bank of directional filters, and the spatial organization is used to perform the detection and generate a binary net mask. In the final step, a binary label indicating "with or without pigmented network" is attributed to each image after extracting topological features to train the AdaBoost classifier.

Recently, Arroyo and Zapirain[33] also proposed an approach for pigmented network detection based on supervised machine learning and structural analysis. The machine learning process was conducted to obtain pixel candidates to create the network by extracting and selecting color, spectral, and statistical texture features, followed by the construction of a classification model. In the structural analysis, a reticular structure detection process is conducted with the aim of establishing whether the image has a pigmented network or not. If the network is present, then the corresponding mask is obtained.

In this paper, an approach oriented toward detection of reticular pattern using texture features is presented to classify dermoscopic skin lesions "with or without reticular pattern." The algorithm is validated on a dataset of 104 dermoscopy images from the database "Derm101."[34]

3 Proposed Methodology

Color and texture features are the two main groups of characteristics used by dermatologists to differentiate skin melanocytic patterns.

Dermoscopic structures, such as reticular pattern and streaks, can be described by texture features, because these markers represent the spatial intensities in an image, allowing the identification of different shapes. Textural features and texture analysis methods can be divided into several categories: statistical, structural, model based, and signal processing based.[35] In

pigmented networks, detection commonly uses statistical and structural approaches.

Statistical methodologies define texture in terms of local graylevel statistics as a function of its pixel inner variability. Structural texture models identify the basic pattern to allocate to a texture arrangement. Statistical features represent a measure of graylevel variations correlated with pixel neighborhood, and structural features explicitly characterize textural properties, such as size and shape.[28]

Detailed and systematic observation of a melanocytic lesion allows the identification of some characteristics whose presence or absence is crucial to diagnosis. Among them is the reticular pattern. Many benign lesions have large areas without a reticular pattern. Other benign lesions, such as congenital pseudomelanoma, can be a particular clinical dilemma (see Fig. 1). This type of congenital nevus is characterized by several to numerous, roundish to oval, dark-brown or black pigmented areas within an otherwise stereotypical congenital nevus, clinically simulating a melanoma within a pre-existing congenital nevus.[24]

The main objective in this work is to detect the presence or absence of reticular patterns regardless of the specific type of lesion. Moreover, with this methodology, the aim is also to obtain high levels of sensitivity and specificity in the automatic classifier by a procedure that does not use preprocessing or image segmentation (as is proposed in the majority of other related methodologies). Good performance in the classifier will contribute to increasing the degree of confidence in the use of computer-aided diagnosis (CAD) techniques in dermatology and to increasing its use in clinical practice as one more clue to the early diagnosis of skin malignancies.

From the variety of possible algorithms, statistical methods of texture feature extraction were applied. In this study, lesions are classified based on image texture features using graylevel co-occurrence matrix (GLCM) and Laws filter masks. The classification system consists of two main processing steps. First, a vector of global texture features is extracted from the image. Next, a simple and efficient classifier/feature selector is built using the AdaBoost learning algorithm to select the best features, in order to discriminate between lesions "with reticular pattern" and lesions "without reticular pattern," and to assign probabilities of being a lesion "with reticular pattern."

3.1 *Image Preprocessing*

In contrast to other methodologies used in dermoscopic machine learning algorithms, the process of detecting and removing artifacts, and the previous segmentation, was avoided in this proposed methodology. As a preprocessing step, the conversion from RGB into a graylevel image was performed by selecting the channel with the highest entropy (as a first-order histogram statistic) in accordance with Ref. 36, then an image resize was applied to a fixed size of 500×600. Each image was then divided into subimages of 100×100.

3.2 *Texture Descriptors*

Feature extraction is the process that extracts higher-level information of an image such as color, shape, and texture. In statistical methods, the features are extracted by computing the neighbor pixel statistics. The basic classical approach consists of the computation of statistics pairs at the neighboring pixels using the GLCM.[37] Mathematically, a co-occurrence matrix is defined over an $M \times N$ image I, parameterized by an offset $(\Delta x, \Delta y)$, as in Eq. (1):

$$\mathrm{GLCM}_{\Delta x,\Delta y}(i,j) = \sum_{m=1}^{M}\sum_{n=1}^{N}\begin{Bmatrix} 1, & \text{if } I(m,n)=i \text{ and if } I(m+\Delta x,\, n+\Delta y)=j \\ 0, & \text{otherwise} \end{Bmatrix}, \tag{1}$$

where i and j are the intensity values of the image I and m and n are the spatial positions. The offset $(\Delta x, \Delta y)$ depends on the direction used and the distance at which the matrix is computed $d(\Delta x, \Delta y)$.

This matrix stores the relative frequencies of graylevel pairs of pixels at a certain relative displacement and can be used to compute several statistics, which will be the elements of the feature vector. The results, presented in this work, were obtained using 10 of the most commonly used statistics that are extracted from the co-occurrence matrix: contrast, correlation, homogeneity, energy, entropy, cluster prominence, cluster shade, inverse difference moment, variance, and difference entropy. As the performance of the classification system is dependent on the number of gray levels used and also on the orientation of the nearest neighbors, the outcome of these features is related to the GLCM.[38] Therefore, several values of graylevels and two ways of combining the orientations (namely, average GLCM versus four GLCM) were tested.

There are, in the literature, many filter banks, and among those, the well-known Laws methodology[39] was chosen to use. The Laws method enrolls filter masks to extract secondary features from natural microstructure characteristics of the image (level, edge, spot, and ripple), which can then be used for segmentation or classification. These masks can have a dimension of 3×3, 5×5, or 7×7 resulting from the convolution from two of the three, five, or seven possible one-dimensional (1-D) kernels, respectively. These masks enable the extraction of structural components of the image when convolved with a textured image.[39] The 14 vectors are shown in Fig. 2.

After the convolution with above-mentioned Laws masks, the outputs are passed to texture energy measurement (TEM) filters for the analysis of the texture properties of each pixel. This step consists of a moving nonlinear window operation, where every pixel of the image is replaced by comparing the pixel with its local neighborhood, based on three statistical

$$\begin{aligned}
L3 &= [\ 1\ \ 2\ \ 1\ ] \\
E3 &= [\ 1\ \ 0\ \ -1\ ] \\
S3 &= [\ 1\ \ -2\ \ 1\ ] \\
L5 &= [\ 1\ \ 4\ \ 6\ \ 4\ \ 1\ ] \\
E5 &= [\ -1\ \ -2\ \ 0\ \ 2\ \ 1\ ] \\
S5 &= [\ -1\ \ 0\ \ 2\ \ 0\ \ -1\ ] \\
R5 &= [\ 1\ \ -4\ \ 6\ \ -4\ \ 1\ ] \\
W5 &= [\ -1\ \ 2\ \ 0\ \ -2\ \ 1\ ] \\
L7 &= [\ 1\ \ 6\ \ 15\ \ 20\ \ 15\ \ 6\ \ 1\ ] \\
E7 &= [\ -1\ \ -4\ \ -5\ \ 0\ \ 5\ \ 4\ \ 1\ ] \\
S7 &= [\ -1\ \ -2\ \ -1\ \ 4\ \ 1\ \ -2\ \ -1\ ] \\
W7 &= [\ -1\ \ 0\ \ 3\ \ 0\ \ -3\ \ 0\ \ 1\ ] \\
R7 &= [\ 1\ \ -2\ \ -1\ \ 4\ \ -1\ \ -2\ \ 1\ ] \\
O7 &= [\ -1\ \ 6\ \ -15\ \ 20\ \ -15\ \ 6\ \ -1\ ]
\end{aligned}$$

Fig. 2 One-dimensional Laws masks of size 3, 5, and 7.

descriptors (mean, absolute mean, and standard deviation). These descriptors are computed according to Eq. (2):

$$\text{Mean} = \frac{\sum_W(\text{neighboring pixels})}{W},$$
$$\text{Absolute mean} = \frac{\sum_W \text{abs}(\text{neighboring pixels})}{W},$$
$$\text{Standard deviation} = \sqrt{\frac{\sum_W(\text{neighboring pixels-mean})^2}{W}}, \tag{2}$$

where W is the window size. The operation will lead to the creation of three TEM images corresponding to each statistical descriptor. Subsequently, for each TEM image, three statistics, namely absolute mean (ABSM), energy, and entropy, will be computed according to Ref. 40 and defined by Eq. (3):

$$\text{ABSM} = \frac{1}{MN}\sum_{i=1}^{M}\sum_{j=1}^{N}|I(i,j)|,$$
$$\text{Energy} = \frac{1}{MN}\sum_{i=1}^{M}\sum_{j=1}^{N}I(i,j)^2,$$
$$\text{Entropy} = \frac{1}{MN}\sum_{i=1}^{M}\sum_{j=1}^{N}I(i,j) - \log\left[I(i,j)\right], \tag{3}$$

where $I(i,j)$ is the pixel value from image I, and M and N are the image dimensions.

All the possible combinations of 1-D kernels were considered, i.e., all Laws masks were applied, and the three statistical descriptors (mean, absolute mean, and standard deviation) were used to determine the TEM images. Next, three amplitude features (ABSM, energy, and entropy) were computed for each obtained TEM. Consequently, there are nine different convolutions for 3×3 masks (denoted as L3), 25 different convolutions for 5×5 masks (denoted as L5), and 36 different convolutions for 7×7 masks (denoted as L7). Three amplitude features for each were then obtained.

3.3 *Feature Selection and Classification*

Using a set of texture features and a training set containing 840 subimages, a number of machine learning approaches could be used to create a binary classifier. However, in this work, the approach has to use a classifier that, during the training phase, automatically selects only those features that are most useful in the discrimination between lesions with or without reticular pattern. Note that the classifier does not know if any particular feature is discriminative or not, so the feature selection is indeed an important part of the learning process. To achieve this aim, the approach presented in Ref. 36 was adapted by using the variant methodology proposed in Ref. 41 of the AdaBoost algorithm,[42] by simultaneously selecting the best features and training the classifier.

Generally, the AdaBoost classifier selects a small subset from the initial set, called weak classifiers, and combines the selected algorithms into a strong, well-performing classifier. For more details regarding the boosting technique, please see Ref. 43, where the original methodology was presented. The variant of the AdaBoost algorithm used in this paper identifies weak classifiers with texture features.

4 Experimental Results and Discussion

In this section, a summary of the conducted experiments and results are shown. The previously presented methodology was evaluated using a dataset of 228 subimages obtained from 55 images. For training and validation purposes, each image was labeled as with or without reticular pattern (ground truth label). These images were taken from the database Derm101[34] and were obtained by dermatologists during clinical exams. All images were stored in JPEG format.

The performance was evaluated for each type of feature: GLCM (T_G), Laws (T_L), and both GLCM and Laws ($T_G + T_L$). The metric evaluations used were sensitivity (SE), specificity (SP), and accuracy (Q).

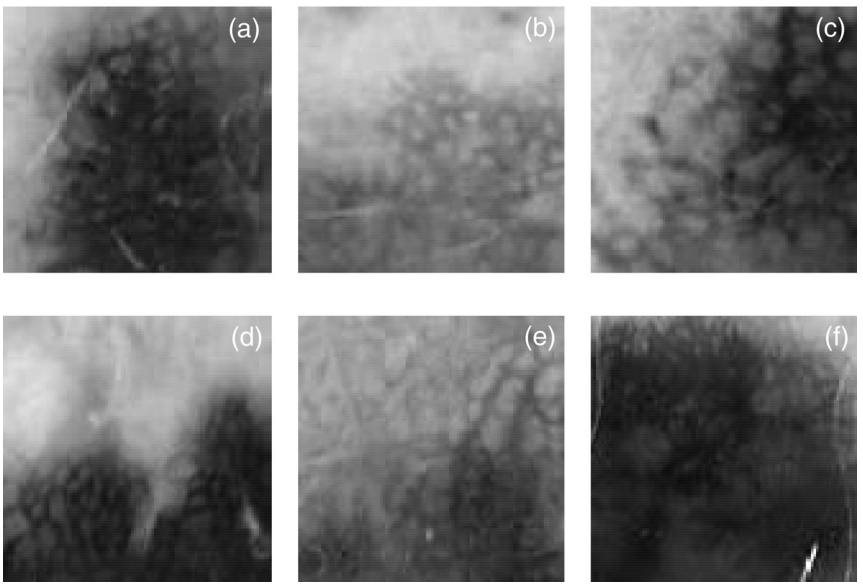

Fig. 3 Result of reticular pattern finder using graylevel co-occurrence matrix (GLCM) and Laws features. (a and d) Clark nevi, (b and e) congenital pseudomelanoma, and (c and f) melanoma.

Two experiments were conducted. In the first experiment, a comparison between the graylevels was computed and the distance parameter of GLCM was optimized. Regarding this, it was acknowledged that the best results were obtained with 256 values of graylevels (G), four orientations, and one distance. These results were not as successful as those noted for the Laws algorithm. The second experiment consisted of determining which of the Laws energy filters produces better results. Three filters—L3, L5, and L7—with 9×9, 11×11, 13×13, 15×15, 17×17, 19×19, and 21×21 window sizes, were used, and for each one of them, one of the best individual results was combined with the best result of the others. The results obtained with the Laws method were quite promising. From these outcomes, the best one (90.16% SE) was chosen, obtained with the combination of the features L3 with 13×13 and L5 with 17×17. Figure 3 shows several examples in which the reticular pattern was detected by the algorithm. In the left column, two subimages of Clark nevi are shown; in the middle column, two subimages of congenital pseudomelanoma are displayed; and in the right column, two subimages of melanoma are presented.

The comparison between the performance of the various mask sizes and the combination of features on the subimages in terms of true detection rate and percentage of error is presented in Figs. 4–7.

Table 1 shows the best combination of features for lesion classification.

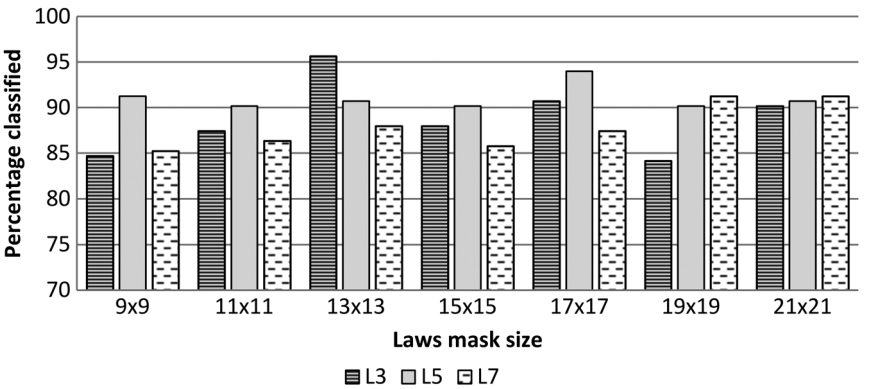

Fig. 4 Performance of Laws masks of different sizes on test set (percentage classified correctly).

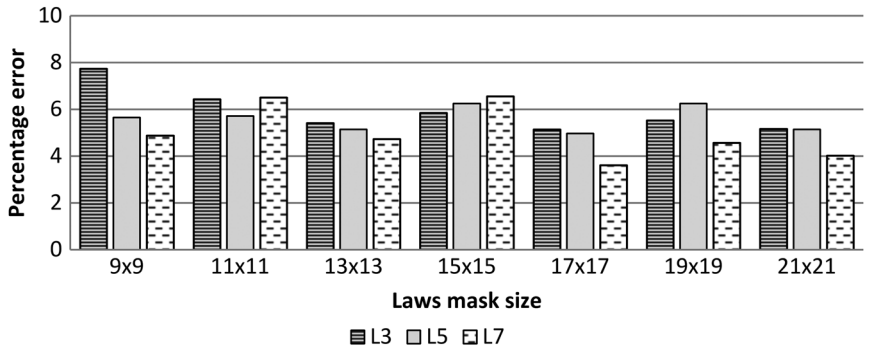

Fig. 5 Performance of Laws masks of different sizes on test set (percentage error).

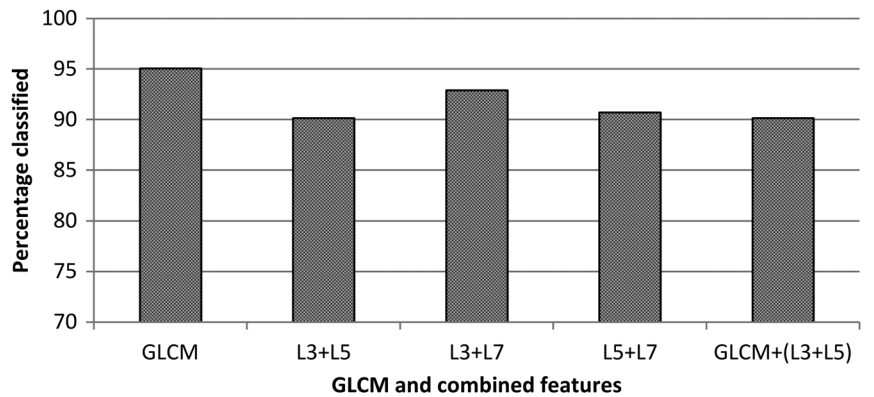

Fig. 6 Performance of GLCM, combined Laws features, and combined GLCM and Laws features on test set (percentage classified correctly).

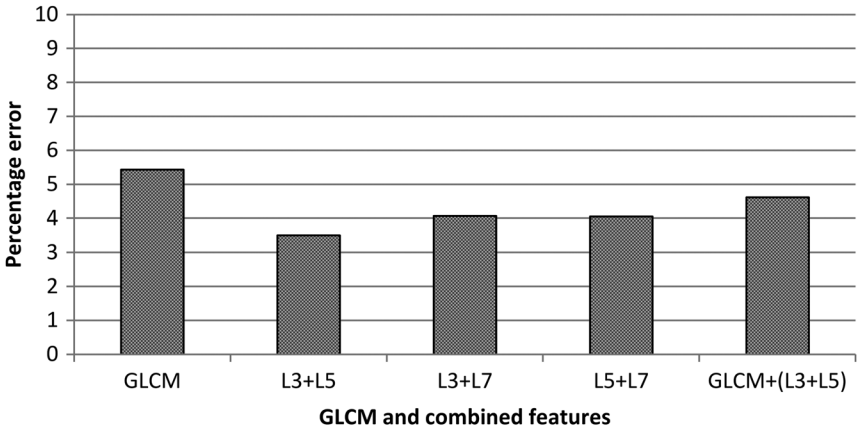

Fig. 7 Performance of GLCM, combined Laws features, and combined GLCM and Laws features on test set (percentage error).

Table 1 Best classification results.

Feature type	SE (%)	SP (%)	Q (%)	Features parameter	Classifier parameter
T_G	95.08	77.78	91.67	$G = 256$; $\theta = 4$	$K = 22$
T_{L3}	90.71	80.00	88.60	$W_3 = 17$	$K = 40$
T_{L5}	93.99	80.00	91.23	$W_5 = 17$	$K = 120$
T_{L7}	87.43	86.67	87.28	$W_7 = 17$	$K = 120$
$T_{L3} + T_{L5}$	90.16	86.67	89.47	$W_3 = 13$; $W_5 = 17$	$K = 120$
$T_{L3} + T_{L7}$	92.90	82.22	90.79	$W_3 = 13$; $W_7 = 21$	$K = 100$
$T_{L5} + T_{L7}$	90.71	84.44	89.47	$W_5 = 17$; $W_7 = 21$	$K = 120$
$T_G + (T_{L3} + T_{L5})$	90.16	82.22	88.60	$G = 256$; $\theta? = 4$; $W_3 = 13$; $W_5 = 17$	$K = 120$

Note: SE, sensitivity; SP, specificity; Q, accuracy.

The detection of reticular patterns fails into the majority of cases when the reticular structures are very tenuous. Regarding the specificity, a score of 86.67% was obtained, identifying the absence of the reticular pattern, even when there was a high presence of hairs and other image artifacts. The algorithm tends to fail when there is a similar texture pattern, as in the case of nonpigmented skin structures similar to this reticular pattern, and also in the presence of too thin or too subtle networks. In these cases, the single use of structural analysis is not enough.

To achieve the real performance of this methodology in dermoscopic images, a comparison with other methods for pigmented network analysis is central [although in the context of machine learning in dermoscopy, it is not easy to find similar methodologies (truly comparable) without using previous segmentation and texture features]. A qualitative assessment of the results is difficult because the outputs, goals, and datasets used can be different.[28,31–33] An empirical comparison can be performed by observing Table 2.

In the presented work, better results are obtained when comparing this study with Anantha et al.[28] in terms of accuracy, Barata et al.[32] in terms of specificity, and Arroyo and Zapirain[33] in terms of both sensitivity and specificity. On the other hand, Sadeghi et al.[31] report a better accuracy value and Barata et al.[32] report a better sensitivity value, omitting the SE and SP values.

Table 2 Results of the most relevant works in the detection of pigmented networks.

	Results			
Work	No. of Images	SE (%)	SP (%)	Q (%)
Anantha et al.[28]	155	—	—	80.00
Sadeghi et al.[31]	500	—	—	93.40
Barata et al.[32,36]	200	91.10	82.10	—
Arroyo and Zapirain[33]	220	86.00	81.67	—
Machado et al. (proposed)	104	90.16	86.67	89.47

5 Conclusion

Reticular patterns are an important inkling in dermoscopic images, and the GLCM and LEM proved to be successful

approaches for their detection. Nevertheless, the Laws methodology has shown a high degree of reliability and has given encouraging results: 90.16% sensitivity, 86.67% specificity, and 89.47% accuracy. The proposed methodology establishes an algorithm to be applied on the original image (avoiding previous preprocessing and segmentation tasks) that is robust against the presence of common artifacts in dermoscopy, such as hairs, air bubbles, or light reflection.

In recent years, the research related to automatic classifiers in medicine, used as an aid to diagnosis (CAD), has had a significant expression in several medical areas, including dermatology. Today, the big challenge is focused on improving the adherence of physicians to these methods, in which quantification is independent of human vision subjectivity.

The results presented here are a very encouraging move toward a robust classifier with several categories of features in order to perform an automatic classification that truly constitutes an aid to clinical practice in everyday life. Beyond the lack of a previous preprocessing step in the image, this work presents the compromise between methodology and its results as the main contribution.

Future work should rely on applying this algorithm to a large dataset composed of images from different origins obtained by different acquisition setup (for comparison purposes). Furthermore, due to its properties, Laws filters can be used to detect other dermoscopic structures, such as dots, or to distinguish melanoma from nonmelanoma lesions. This approach will be tested in the near future.

Acknowledgments

This work was supported in part by project DERMCALSS, grant Nos. CENTRO-07-ST24-FEDER-002022 and PEst-OE/EEI/LA0008/2013.

References

1. D. L. Kasper and R. H. Tinsley, *Harrison's Principles of Internal Medicine*, McGraw-Hill Companies, Inc., New York (2005).
2. D. C. Whiteman, W. J. Pavan, and B. C. Bastian, "The melanomas: a synthesis of epidemiological, clinical, histopathological, genetic, and biological aspects, supporting distinct subtypes, causal pathways, and cells of origin," *Pigment Cell Melanoma Res.* **24**, 879–897 (2011).
3. I. Zalaudek et al., "How to diagnose nonpigmented skin tumors: a review of vascular structures seen with dermoscopy: part I. Melanocytic skin tumors," *J. Am. Acad. Dermatol.* **63**, 361–374 (2010); quiz 375-366.
4. S. W. Menzies, C. Ingvar, and W. H. McCarthy, "A sensitivity and specificity analysis of the surface microscopy features of invasive melanoma," *Melanoma Res.* **6**, 55–62 (1996).
5. L. Andreassi et al., "Digital dermoscopy analysis for the differentiation of atypical nevi and early melanoma: a new quantitative semiology," *Arch Dermatol.* **135**, 1459–1465 (1999).
6. D. Piccolo et al., "Dermoscopic diagnosis by a trained clinician vs. a clinician with minimal dermoscopy training vs. computer-aided diagnosis of 341 pigmented skin lesions: a comparative study," *Br. J. Dermatol.* **147**, 481–486 (2002).
7. R. Fonseca-Pinto and A. Andrade, "Image empirical mode decomposition (IEMD) in dermoscopic images: artefact removal and lesion border detection," in *Proc. Signal Processing Pattern Recognition and Applications*, pp. 341–345 (2010).
8. J. Pereira and R. Fonseca-Pinto, "Segmentation strategies in dermoscopy to follow-up melanoma: combined segmentation scheme," *J. Sci. Technol.* **5**(3), 56–61 (2015).
9. Q. Abbas et al., "Lesion border detection in dermoscopy images using dynamic programming," *Skin Res. Technol.* **17**, 91–100 (2011).
10. Q. Abbas, I. Fondon, and M. Rashid, "Unsupervised skin lesions border detection via two-dimensional image analysis," *Comput. Methods Programs Biomed.* **104**, e1–e15 (2011).
11. A. Afonso and M. Silveira, "Hair detection in dermoscopic images using percolation," in *Conf. Proc. IEEE Eng. Med. Biol. Soc.* (2012).
12. H. P. Soyer et al., "Diagnostic reliability of dermoscopic criteria for detecting malignant melanoma," *Dermatology* **190**, 25–30 (1995).
13. A. Blum, G. Rassner, and C. Garbe, "Modified ABC-point list of dermoscopy: a simplified and highly accurate dermoscopic algorithm for the diagnosis of cutaneous melanocytic lesions," *J. Am. Acad. Dermatol.* **48**, 672–678 (2003).
14. E. Savk et al., "Interobserver agreement in the use of the ABCD rule for dermoscopy," *J. Dermatol.* **31**, 1041–1043 (2004).
15. I. Zalaudek et al., "Three-point checklist of dermoscopy: an open internet study," *Br. J. Dermatol.* **154**, 431–437 (2006).
16. G. Argenziano et al., "Seven-point checklist of dermoscopy revisited," *Br. J. Dermatol.* **164**, 785–790 (2011).
17. Q. Abbas et al., "Lesion border detection in dermoscopy images using dynamic programming," *Skin Res. Technol.* **17**, 91–100 (2011).
18. D. Piccolo et al., "Computer-automated ABCD versus dermatologists with different degrees of experience in dermoscopy," *Eur. J. Dermatol.* **24**(4), 477–481 (2014).
19. Z. Liu et al., "Distribution quantification on dermoscopy images for computer-assisted diagnosis of cutaneous melanomas," *Med. Biol. Eng. Comput.* **50**, 503–513 (2012).
20. B. Cheng et al., "Analysis of clinical and dermoscopic features for basal cell carcinoma neural network classification," *Skin Res. Technol.* **19**, e217–e222 (2013).
21. M. A. Paradiso and T. Carney, "Orientation discrimination as a function of stimulus eccentricity and size: nasal/temporal retinal asymmetry," *Vision Res.* **28**, 867–874 (1988).
22. V. P. Zworykin, "Neuromorphological evidence of individual differences in human vision," *Arkh Anat Gistol Embriol.* **81**(10), 21–24 (1981).
23. J. T. Yates et al., "Contrast sensitivity: Characteristics of a large young adult population," *Am. J. Optom. Physiol. Opt.* **64**, 519–527 (1987).
24. "Dermoscopy tutorial," 2003, http://www.dermoscopy.org/atlas/base.html (accessed 2014).
25. R. H. Johr, "Dermoscopy: alternative melanocytic algoritms-the ABCD rule of dermatoscopy, menzies scoring method and 7-point checklist," *Clin. Dermatol.* **20**(3), 240–247 (2002).
26. C. Dolianitis, J. Kelly, and P. Simpson, "Comparative performance of 4 dermoscopic algorithms by nonexperts for the diagnosis of melanocytic lesions," *Arch. Dermatol.* **141**(8), 1008–1014 (2005).
27. M. Fleming et al., "Techniques for a structural analysis of dermatoscopic imagery," *Comput. Med. Imaging Graphics* **22**, 375–389 (1998).
28. M. Anantha, R. Moss, and W. Stoecker, "Detection of pigment network in dermatoscopy images using texture analysis," *Comput. Med. Imaging Graphics* **28**, 225–234 (2004).
29. G. Betta et al., "Dermoscopic image-analysis system: Estimation of atypical pigment network and atypical vascular pattern," in *Proc. Int. Workshop Medical Measurement and Applications* (2006).
30. G. D. Leo et al., "Automatic diagnosis of melanoma: a software system based on the 7-point checklist," in *Proc. 43rd Hawaii Int. Conf. System Sciences* (2010).
31. M. Sadeghi et al., "A novel method for detection of pigment network in dermoscopic images using graphs," *Comput. Med. Imaging Graphics* **35**, 137–143 (2011).
32. C. Barata, J. Marques, and J. Rozeira, "A system for the detection of pigment network in dermoscopy images using directional filters," *IEEE Trans. Biomed. Eng.* **59**, 2744–2754 (2012).
33. J. G. Arroyo and B. G. Zapirain, "Detection of pigment network in dermoscopy images using supervised machine learning and structural analysis," *Comput. Biol. Med.* **44**, 144–157 (2014).
34. "DERM101," http://www.derm101.com (accessed 2014).
35. M. Tuceryan and A. K. Jain, "Texture analysis," in *The Handbook of Pattern Recognition and Computer Vision*, 2nd ed., C. H. Chen, L. F. Pau, and P. S. P. Wang, Eds., pp. 207–248, World Scientific Publishing Co. (1998).
36. C. Barata et al., "Two systems for the detection of melanomas in dermoscopy images using texture and color features," *IEEE Syst. J.* **8**, 965–979 (2014).

37. R. Haralick, K. Shanmugam, and I. Dinstein, "Textural features for image classification," *IEEE Trans. Syst. Man Cybern.* **2**, 610–621 (1973).
38. D. Clausi, "An analysis of co-occurrence texture statistics as a function of grey level quantization," *Can. J. Remote Sens.* **28**(1), 45–62 (2002).
39. K. Laws, *Textured Image Segmentation*, Image Processing Institute, University of southern California, Los Angeles, California (1980).
40. H. A. Elnemr, "Statistical analysis of Law's mask texture features for cancer and water lung detection," *Int. J. Comput. Sci.* **10**, 196–202 (2013).
41. P. Viola and M. J. Jones, "Robust real-time face detection," *Int. J. Comput. Vision* **57**, 137–154 (2004).
42. Y. Freund and R. Schapire, "A decision-theoretic generalization of online learning and an application to boosting," *J. Comput. Syst. Sci.* **55**, 119–139 (1997).
43. Y. Freund and R. E. Schapire, "A short introduction to boosting," *J. Jpn. Soc. Artif. Intell.* **14**(5), 771–780 (1999).

Marlene Machado received her degree in biomedical engineering from the Polytechnic Institute of Bragança—Portugal and an MSc degree in biomedical engineering from the Faculty of Engineering from the University of Porto—Portugal. Currently, she is a researcher in the Instituto de Telecomunicações, Leiria, Portugal.

Jorge Pereira received his MSc in biomedical engineering from the Faculty of Engineering from the University of Porto, Portugal. Currently, he is a researcher in the Instituto de Telecomunicações, Leiria, Portugal.

Rui Fonseca-Pinto is an associate professor at the Polytechnic Institute of Leiria-Portugal and is also a researcher at the Instituto de Telecomunicações (Multimedia Signal Processing Group—Leiria). He received his PhD in biomedical engineering and biophysics from the University of Lisbon-Portugal and obtained a degree in medicine in 2013 from the Faculty of Medicine from the University of Lisbon, Portugal.